AIAA 97-1379

# Experimental Characterization of Hysteresis in a Revolute Joint for Precision Deployable Structures

Mark S. Lake, Jimmy Fung, Kevin Gloss, and Derek S. Liechty
NASA Langley Research Center
Hampton, Virginia

**38th Structures, Structural Dynamics and Materials Conference**

7-10 April 1997
Kissimmee, Florida

# Experimental Characterization of Hysteresis in a Revolute Joint for Precision Deployable Structures

Mark S. Lake*, Jimmy Fung†, Kevin Gloss‡, and Derek S. Liechty†
*NASA Langley Research Center, Hampton, Virginia, 23681-0001*

Recent studies of the micro-dynamic behavior of a deployable telescope metering truss have identified instabilities in the equilibrium shape of the truss in response to low-energy dynamic loading. Analyses indicate that these micro-dynamic instabilities arise from stick-slip friction within the truss joints (e.g., hinges and latches). The present study characterizes the low-magnitude quasi-static load-cycle response of the precision revolute joints incorporated in the deployable telescope metering truss, and specifically, the hysteretic response of these joints caused by stick-slip friction within the joint. Detailed descriptions are presented of the test setup and data reduction algorithms, including discussions of data-error sources and data-filtering techniques. Test results are presented from thirteen specimens, and the effects of joint preload and manufacturing tolerances are investigated. Using a simplified model of stick-slip friction, a relationship is made between joint load-cycle behavior and micro-dynamic dimensional instabilities in the deployable telescope metering truss.

## Nomenclature

| | |
|---|---|
| $c$ | = viscous damping parameter |
| $F$ | = load parameter |
| $F_{cr}$ | = load at which slippage occurs |
| $k_1$, $k_2$, $k_3$ | = stiffness parameters |
| $m_1$, $m_2$ | = mass parameters |
| $\mu N$ | = Coulombic friction parameter |
| $x_1$, $x_2$ | = displacement parameters |

## Introduction

NASA's Office of Space Science has recently inaugurated the Astronomical Search for Origins and Planetary Systems (Origins) Program. Between the years 2005 and 2010, this program will launch a series of extraordinary new science instruments including the Next Generation Space Telescope (NGST, Fig. 1). The success of these revolutionary science instruments, and the success of the Origins Program, depends on the development of many new materials and structures technologies.[1] One key technology which is required by all planned Origins science instruments is sub-micron-stable deployable structures.

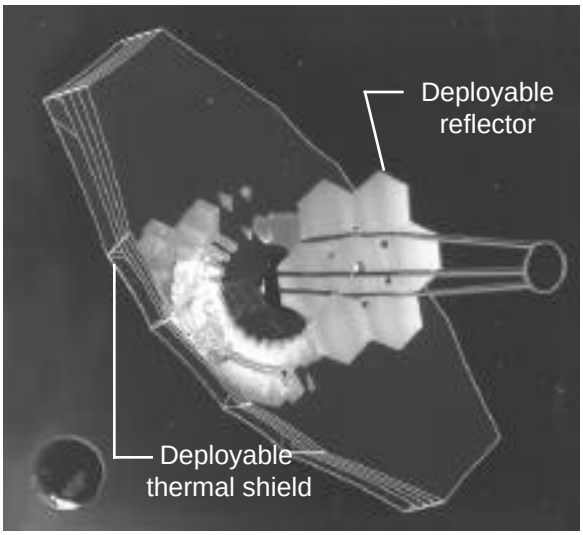


**Fig. 1 NGST concept.**

Nonlinear mechanical response within deployment mechanisms (i.e., joints) is the fundamental limitation to post-deployment dimensional stability in a mechanically deployable structure.[2] The recently developed revolute (i.e., hinge) joint shown in Fig. 2 has been shown to exhibit response to cyclic loading that is very nearly linear with a small amount of hysteresis attributed to friction-induced micro-slippage.[3] Testing of a prototype deployable telescope metering truss that incorporates these new joints has demonstrated that the structure exhibits micro-dynamic instabilities in its equilibrium shape that are also attributed to friction-induced micro-slippage in the joints.[4]

---

*Senior Research Engineer, Structural Mechanics Branch, Senior Member AIAA.
† Cooperative Education Student, Student Member AIAA.
‡ Langley Aerospace Research Summer Scholar.

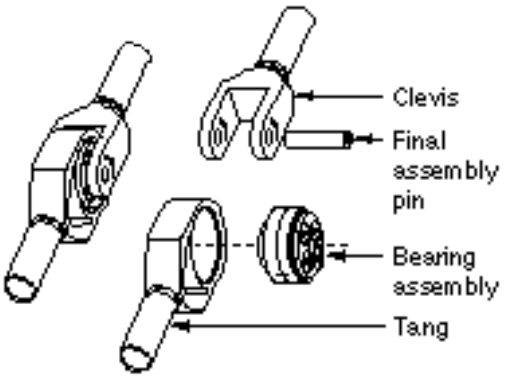


**Fig. 2a Linear revolute joint diagram.**

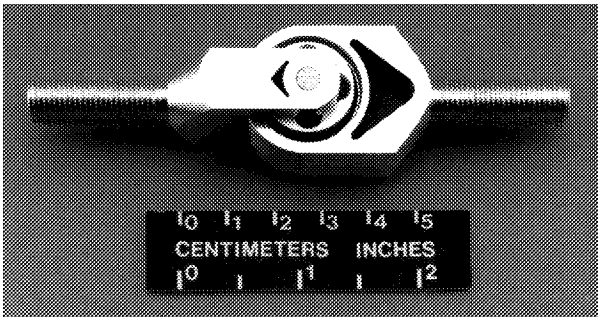


**Fig. 2b Linear revolute joint photograph.**

The present paper will present test results that identify critical features in the hysteretic response of the highly-linear revolute joint and correlate these hysteretic-response features with the micron-level dimensional instabilities observed in the prototype deployable telescope metering truss. Identifying this connection between load-cycle hysteresis in the joints and micron-level dimensional instabilities in the structure is one significant step towards enabling the design of mechanically deployable structures for optical science instruments.

## Background

The revolute joint shown in Fig. 2 was designed to exhibit minimal nonlinear response to load cycling, as it is believed that load-cycle response nonlinearities in deployment mechanisms are responsible for dimensional instabilities in deployable structures.[3] The design represents a substantial departure from conventional pin-clevis joints in which clearance between the pin and the joint tang allows rotation of the joint halves. Instead, the present design incorporates a precision preloaded angular-contact ball bearing to enable rotation, and a slightly over-sized pin which is press-fit into the bearing assembly and joint clevis as a means of final assembly of the joint halves. The bearing is internally preloaded to eliminate freeplay, and the bearing diameter is maximized to minimize stiffness changes due to nonlinear interface conditions between the balls and the races. The pin is press-fit to minimize nonlinear effects at the pin-to-clevis and the pin-to-bearing-assembly interfaces. However, load transfer through the bearing and pin involves a small amount of friction slippage at the interfaces that can lead to micro-dynamic dimensional instabilities in structures incorporating the joint.

### Micro-dynamic Testing of a Prototype Deployable Telescope Metering Truss

Reference 5 presents results from tests of a deployable telescope metering truss which incorporates four precision revolute joints and one end-of-deployment latch joint, as shown in Fig. 3. This test article represents a portion of the metering truss that would support one reflector panel in a segmented telescope mirror (e.g., one of the six perimeter panels shown in Fig. 1). Results from micro-dynamic testing of this structure indicate that the structure exhibits changes in its equilibrium shape following transient disturbances. This phenomenon is referred to as “micro-lurching”.

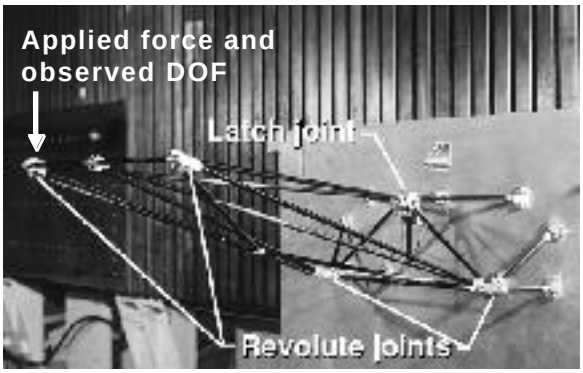


**Fig. 3 Precision reflector metering truss fabricated with linear revolute joints.**

### Stick-Slip Friction Model of Micro-Lurching

Analytical results presented in Ref. 5 from a simple two-degree-of-freedom model suggest that micro-lurching is an artifact of stick-slip instability due to load transfer through friction. Since both the revolute joints and the latch joint possess mechanical interfaces at which load is partially transferred through friction, it seems plausible that these mechanisms are responsible for micro-lurching in the deployable telescope metering truss.

The simplified model used in Ref. 5 is shown schematically in Fig. 4 with model parameters described in Fig 4a. In these analyses, the simplified model was used to simulate the dynamic response of the deployable telescope metering truss in the single degree of freedom shown in Fig. 3 (i.e., vertical motion of an outboard

joint). The parameters of the simplified model represented modal parameters of the truss (e.g., modal masses and stiffnesses) rather than physical parameters of the truss (e.g., member masses and stiffnesses). For these dynamic-response analyses, the model can be interpreted to represent a linear oscillator coupled with a nonlinear oscillator as shown in Fig. 4b. The nonlinear oscillator exhibits stick-slip instabilities due to the Coulombic friction element. These instabilities give rise to micro-lurch motion in the total system response ("Observed DOF" in Figs. 3 and 4).

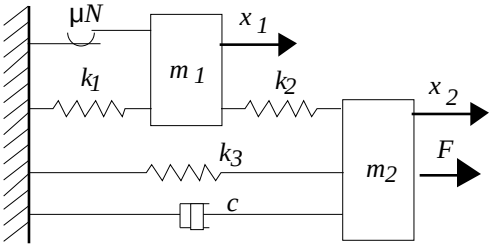


**a) Model parameters**

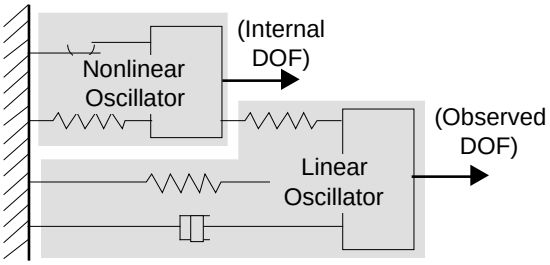


**b) Dynamic-response interpretation of model**

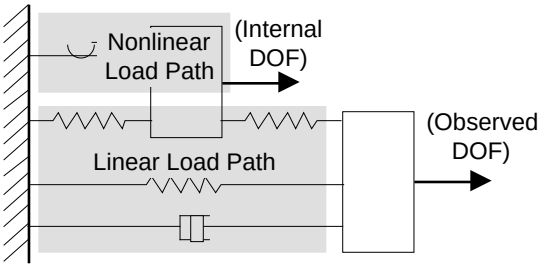


**c) Mechanical-response interpretation of model**

**Fig. 4 Simple system model from Ref. 5.**

The analyses presented in Ref. 5 using this model closely agree with the extensive experimental data also presented in Ref. 5 on the micro-lurching response of the deployable telescope metering truss. These analyses reinforced laboratory findings that micro-lurching is chaotic (i.e., exhibits statistical variability which is highly dependent on initial conditions), and micro-lurching is an instability response dependent on excitation energy. The good correlation between experiment and analyses presented in Ref. 5 strongly supports the presumption that micro-lurching is caused by stick-slip interactions within the structure.

### Stick-Slip Friction Model of Hysteresis in Quasi-Static Load-Cycle Response

The simplified model presented in Fig. 4 can also be used to gain insight into the response of the deployable telescope metering truss under quasi-static load cycling. For this type of mechanical-response analysis, the model can be interpreted to represent two parallel load paths: one linear and viscoelastic; and one nonlinear and Coulombic (as shown in Fig. 4c). Friction slippage in the nonlinear load path can result in hysteretic response to quasi-static load cycling. Referring to Fig. 4a, it can be shown that the critical load-cycle magnitude above which friction slippage occurs is:

$$F_{cr} = \frac{\mu N \left(k_2 + k_3\right)}{k_2} \qquad (1)$$

Conversely, the simplified model presented in Fig. 4 exhibits no friction slippage, and no hysteresis in response to load cycling for load-cycle magnitudes below $F_{cr}$.

Substituting the best-fit values derived in Ref. 5 for the simplified model parameters (i.e., $\mu N$, $k_2$, and $k_3$) into Eq. (1) gives a value for $F_{cr}$ equal to 6.58 N (1.5 $lb_f$). In other words, the simplified analyses presented in Ref. 5 suggest that the response of the deployable telescope metering truss to quasi-static load cycling should be linear and elastic for load-cycle magnitudes up to 6.58 N (1.5 $lb_f$). Whereas, the quasi-static load cycle response of the deployable telescope metering truss should exhibit some friction-induced hysteresis for load-cycle magnitudes greater than 6.58 N (1.5 $lb_f$).

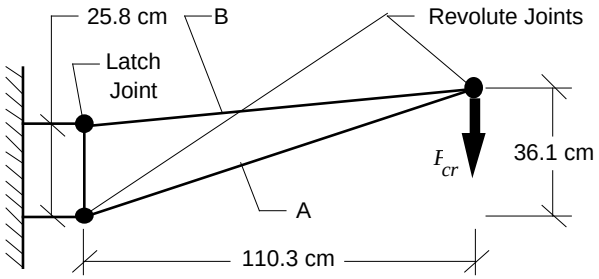


**Fig. 5 Static-loading diagram of deployable telescope metering truss.**

Recall that these analyses predict the response of the deployable telescope metering truss in the single degree of freedom shown in Fig. 3 (i.e., vertical motion of an outboard joint). To relate this global load-cycle-response analysis to the local load-cycle response of individual joints within the truss, consider the static-

loading diagram shown in Fig. 5. It can be shown that a load of magnitude $F_{cr}$ applied at point *C* (i.e., the tip of the truss), results in axial loads in members *A* and *B* of approximately $5F_{cr}$. Hence, a load of 6.58 N (1.5 $lb_f$) applied at the tip of the metering truss results in member loads of approximately 33 N (7.5 $lb_f$). In other words, global load cycling of the metering truss at a magnitude of 6.58 N (1.5 $lb_f$) results in local load cycling of the joints at a magnitude of 33 N (7.5 $lb_f$).

Therefore, the model used in Ref. 5 to predict micro-lurching behavior in the deployable metering truss implicitly assumes that the individual joints in the metering truss exhibit linear elastic response under load cycling up to 33 N (7.5 $lb_f$) in magnitude.

### Previous Load-Cycle Testing of the Joint

Two previous studies have investigated the load-cycling response of the precision revolute joints.[2,3] However, neither of these studies encompassed a range of load-cycle magnitudes sufficient to adequately characterize the hysteretic behavior of the joint.

Bullock[2] conducted extensive testing of the precision revolute joint to characterize its response to low-magnitude, quasi-static, load cycling (i.e., less than 22 N (5 $lb_f$) of load-cycle magnitude). Bullock's data indicate that the precision revolute joint exhibits no significant hysteresis under quasi-static load cycling in this low-load regime. These results suggest that 22 N (5 $lb_f$) of extensional load is not sufficient to cause significant micro-slippage at the interfaces within the joint where load is transferred through friction.

Conversely, results presented in Ref. 3 indicate that the displacement response of the joint exhibits approximately 1% hysteresis under quasi-static extensional load cycling at 222 N (50 $lb_f$) and 445 N (100 $lb_f$) of load-cycle magnitude. These data suggest that friction-induced micro-slippage is significant in the joint at load-cycle magnitudes equal to and exceeding 222 N (50 $lb_f$).

Since it appears that that friction-induced micro-slippage within the joints is responsible for micro-lurching in the structure, it is important to understand how the magnitude of micro-slippage varies with load-cycle magnitude. The present study is intended to characterize the relationship between friction-induced micro-slippage (as evidenced by displacement-response hysteresis) and load-cycle magnitude. In addition, the present study is intended to identify the effects on load-cycle hysteresis of pre-load within the joint's angular-contact bearing and the press-fit of the joint's final assembly pin (see Fig. 2a). These design parameters have been isolated for study because it is believed that they could have a significant effect on the friction-induced micro-slippage that occurs within the joint.

## Description of Tests

### Test Specimens

Thirteen specimens were constructed for load cycle testing in the present tests. Three of the specimens were calibration specimens (C-0, C-a, and C-b), and ten were precision revolute joints (J-a-05, J-b-05, J-a-10, J-b-10, J-a-10, and J-b-10). A summary of these specimens is presented in Table 1.

**Table 1 Test specimens**

| Name | # tested | Pin press-fit* | Bearing preload |
|---|---|---|---|
| C-0 | 1 | N/A | N/A |
| C-a | 1 | a | N/A |
| C-b | 1 | b | N/A |
| J-a-05 | 1 | a | 22-44 N (5-10 $lb_f$) |
| J-b-05 | 1 | b | 22-44 N (5-10 $lb_f$) |
| J-a-10 | 1 | a | 44-66 N (10-15 $lb_f$) |
| J-b-10 | 5 | b | 44-66 N (10-15 $lb_f$) |
| J-a-20 | 1 | a | 89-111 N (20-25 $lb_f$) |
| J-b-20 | 1 | b | 89-111 N (20-25 $lb_f$) |

*Difference between pin and hole diameters: 0.069 - 0.089 mm (0.0027 - 0.0035 in) for "a" press-fit ; and 0.043 - 0.064 mm (0.0017 - 0.0025 in) for "b" press-fit.

One of the calibration specimens (C-0) was a solid aluminum rod sized to exhibit approximately the same axial stiffness as the joint specimens. Due to its highly linear and non-hysteretic response to load cycling, this specimen was used to verify operation of the test apparatus and data reduction system. The remaining two calibration specimens (C-a and C-b) were identical to the precision revolute joint specimens except the bearing assembly (see Fig. 2a) was replaced with a solid piece of aluminum machined to the same outer dimensions as the bearing assembly. These calibration specimens were used to isolate the effects on load-cycle response of the final assembly pin.

The remaining specimens were all precision revolute joints possessing various bearing preloads and pin press-fits as summarized in Table 1. The bearing preload is the lateral force which compresses the matched pair of angular contact bearings together in the bearing assembly. Due to manufacturing tolerances, the bearing preload is specified as a range of values rather than a single value. Details on the design of the bearing assembly and the mechanism which provides the preload force are presented in Ref. 3. Three bearing preload ranges were tested in the present study: 22-44; 44-66; and 89-111 N (5-10; 10-15; and 20-25 $lb_f$; respectively).

The final-assembly-pin press-fit is determined by the relative diameters of the pin (which is slightly over-sized) and the holes in the joint clevis and bearing

assembly that accept the pin. The “a” press-fit corresponds to a pin which is between 0.069 mm and 0.089 mm (0.0027 in. and 0.0035 in., respectively) larger in diameter than the holes. The “b” press-fit corresponds to a pin which is between 0.043 mm and 0.064 mm (0.0017 in. and 0.0025 in., respectively) larger in diameter than the holes. Therefore, the “a” press-fit is heavier than the “b” press-fit resulting in higher interface stresses between the pin and the holes.

**Test Setup**

The joints were load-cycle tested using a 4.45 kN (1 kip) -capacity tension-compression test machine (see Fig. 6). Total center-line displacement across the specimen was inferred by averaging displacement measurements from two fiber-optic displacement transducers as shown in Fig. 7, and total axial load was measured using a 1 kN (225 $lb_f$) -capacity, tension-compression load cell mounted within the load frame. Load and displacement data were converted from analog to digital form using a 16-bit analog-to-digital converter card in a personal-computer-based data acquisition and reduction system.

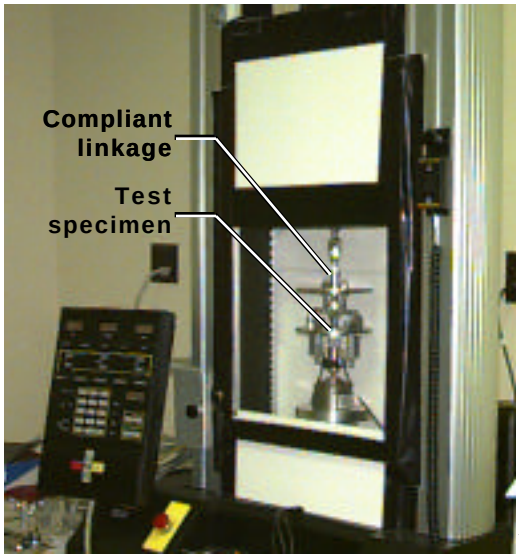


**Fig. 6 Axial load-cycle test setup.**

To minimize off-axis loading of the specimen (e.g., lateral shear and bending) arising from misalignment in the test apparatus, a compliant linkage was inserted between the test specimen and the crosshead of the load frame (above the specimen in Fig. 6). This compliant linkage was constructed using three revolute joints identical to the test specimens. The hinge axes of the test specimen and the joints in the compliant linkage were oriented such that no lateral moments or shear forces could be transferred between the test specimen and the load frame crosshead.

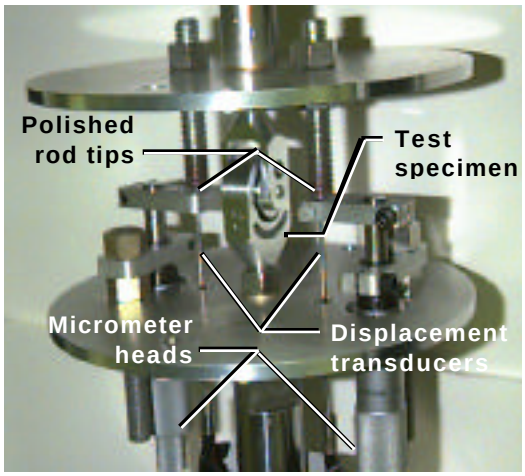


**Fig. 7 Test specimen assembly.**

**Instrumentation and Test Procedure**

Great care was taken to minimize noise and hysteresis in the load and displacement instrumentation in order to ensure accurate characterization of the hysteretic response of the specimens. In particular, fiber-optic displacement transducers were selected instead of electro-mechanical displacement transducers (e.g., LVDT’s) because the fiber-optic instruments exhibit no hysteresis in their response. The load cell was calibrated prior to testing and its response was determined to be linear to within 0.034% of full scale while exhibiting only 0.036% hysteresis relative to full scale. This small amount of load-cell hysteresis was found to be insignificant.

The test specimen was mounted between two circular plates which served as reference planes for displacement measurements (see Fig. 7). The two displacement transducers were located adjacent to the specimen and equidistant from the specimen center-line. Center-line displacement of the specimen was inferred by averaging the displacement measurements from the two displacement transducers. To minimize displacement-measurement errors arising from lateral bending of the specimen, the displacement transducers were located as close to the center-line of the specimen as possible, and the tips of the displacement transducers were located midway between the measurement plates (i.e., along the hinge axis of the specimen).

The displacement transducers were mounted to the bottom plate using micrometer heads (see Fig. 7) to allow vernier positioning of the transducer tips. Two threaded rods attached to the upper plate were positioned such that their polished ends were in line with the tips of the displacement transducers. These polished rod

ends reflected the light emitted by the displacement transducers.

The displacement transducers exhibit a linear response over a displacement range of approximately 50 microns (0.002 in). Within this range, it is possible to convert transducer voltage to tip displacement by multiplying voltage by a calibration constant. Outside of this linear-response range, the voltage-displacement response of the transducers is nonlinear, but very repeatable. It was determined that much of the testing required more than 50 microns (0.002 in) displacement response range. Therefore, analytical calibration functions were derived from accurate calibration data to describe the nonlinear voltage-displacement response of the transducers. These nonlinear calibration functions were applicable over a displacement range of approximately 100 microns (0.004 in).

Prior to testing, each specimen was installed into the test machine and the displacement transducers were aligned as described previously. The displacement transducers were turned on at least 30 minutes before taking any data to allow them to warm-up and stabilize. To minimize drifting of the displacement signals due to shifting air currents and thermal transients, the test cell was enclosed in thin fiber-board insulation material with a plexi-glass panel to allow viewing of the specimen.

Each test specimen was load cycled between tension and compression load limits of: 44.5; 66.8; 89.0; 111.3; 133.5; 178.0; 222.5; 267.0; 356.0; and 445.0 N (10, 15, 20, 25, 30, 40, 50, 60, 80, and 100 $lb_f$). To generate statistically significant results, each specimen was tested six times at most load-cycle magnitudes (only four tests were conducted on each specimen at each of the highest two load-cycle magnitudes). During each test, displacement and load data were collected through three complete load cycles of the specimen between the given load-cycle limits.

### Data Reduction Procedure

In real time during each test, the voltage data from the load cell and displacement transducers were converted to raw load and displacement data by applying the appropriate calibration functions. Then, the two displacement readings were averaged to produce a raw total displacement measurement. The resulting raw load and displacement data were written to a data file and reduced after the test was completed. A typical raw load-displacement response is presented in Fig. 8, and the corresponding raw hysteretic response (derived by subtracting the best-fit straight line from the total response) is presented in Fig. 9.

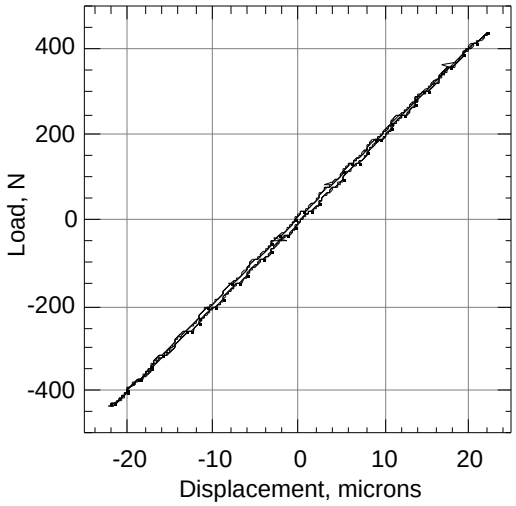


**Fig. 8 Typical raw load-cycle response.**

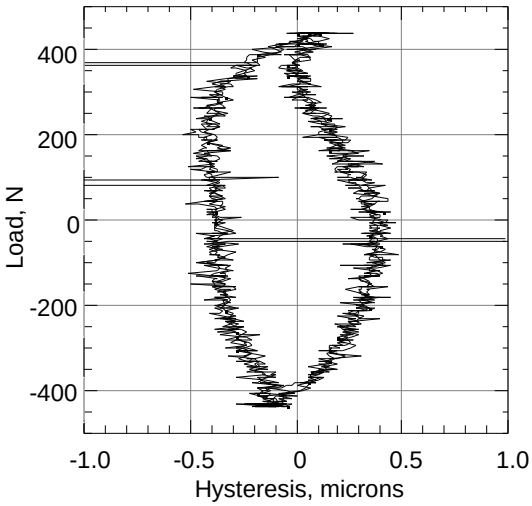


**Fig. 9 Typical raw hysteretic response.**

From Fig. 9 it is apparent that the displacement data possesses more noise than the load data, and this noise is of a high-frequency nature including fairly large-magnitude spikes (e.g., horizontal spikes in Fig. 9). During post-processing, the load and displacement data arrays were first sent through a filter to remove rows of data in which data spikes occurred. Then the data arrays were passed through a second order, forward/backward Butterworth filter to reduce remaining high-frequency noise. The filter used in the present tests was essentially identical to that used by Bullock,[2] and it was chosen because it provided good filtering without introducing significant biasing errors into the data. (Since the study of hysteretic response is, by definition, a survey of time history in data, it is extremely important to avoid data filtering routines that introduce biasing errors.) After filtering the data, the first and last

fifty points in both load and displacement data arrays were removed to eliminate filtering transients.

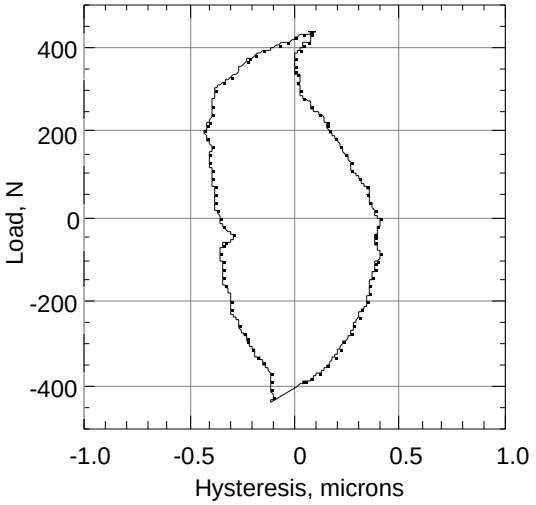


**Fig. 10 Typical filtered hysteretic response.**

Finally, data from the three load cycles were "averaged" into a single load cycle. This averaging was accomplished by partitioning the data into four quadrants defined by the sign of the load (i.e., tension or compression) and sign of the load rate (i.e., increasing or decreasing). After partitioning, the data were sorted by load magnitude, and the four partitioned data sets were recombined into a single "averaged" load cycle. The averaged data were then passed through the forward/backward Butterworth filter once again. The data from Fig. 9 were filtered and averaged and the results are presented in Fig. 10. Comparing Figs. 9 and 10, it can be seen that the data filtering and averaging procedure effectively reduces displacement data noise by more than an order of magnitude.

### Low-Frequency Oscillations in Displacement Transducers

The clearly defined hysteresis loop presented in Fig. 10 demonstrates that the current test setup and data reduction algorithms are capable of characterizing the hysteretic response of the joint specimens at high load-cycle magnitude (i.e., 445N (100 $lb_f$)). Data from the same specimen in response to load-cycling at low magnitude (i.e., 44N (10 $lb_f$)) are presented in Fig. 11. The ordinate and abscissa in Fig. 11 cover only one-tenth of the range of the ordinate and abscissa in Fig. 10. Unlike the results presented in Fig. 10, the hysteresis loop presented in Fig. 11 is poorly defined. In fact, the loop in Fig. 11 exhibits low-frequency waviness with an amplitude of about 25 nm ($1x10^{-6}$ in), and the right and left branches of the loop cross over each other.

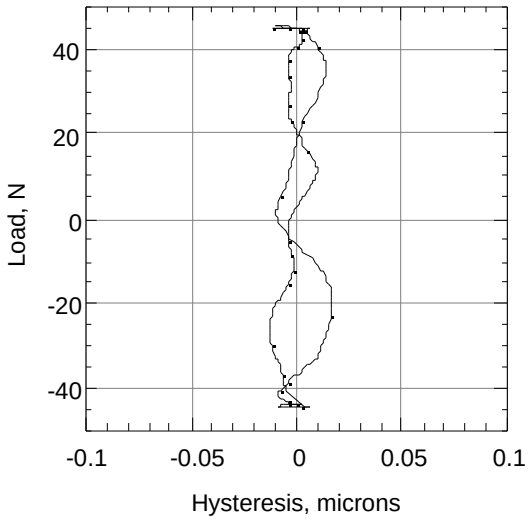


**Fig. 11 Typical filtered hysteretic response at low load-cycle magnitude.**

To determine if this waviness is an artifact of the inherent instabilities in the displacement transducers (e.g., low-amplitude, low-frequency oscillations of the transducer power supply), a control experiment was conducted in which static load and displacement data were taken using the C-0 specimen. In this test, the specimen was held statically at zero load while data were taken in the same way as during a normal load-cycle test. The raw data were passed through the aforementioned data-spike removal algorithm and the forward/backward Butterworth filter to remove high-frequency noise. Time histories of the resulting filtered load and displacement data are presented in Fig. 12.

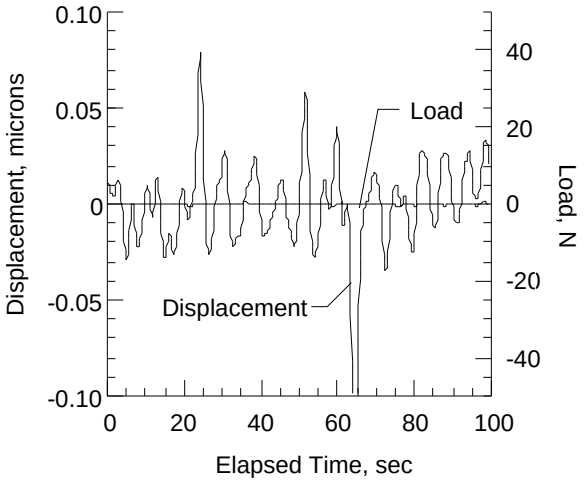


**Fig. 12 Instrumentation instabilities.**

The left-hand ordinate in Fig. 12 corresponds to the displacement data, and the right-hand ordinate corresponds to the load data. The ordinates range

between the same limits as the ordinate and abscissa in Fig. 11. The filtered load data are very stable, maintaining a mean value of zero (exhibiting no discernible drift) throughout the test with a standard deviation of only 0.21 N (0.05 $lb_f$). Although the filtered displacement data also maintained a mean value of approximately zero, the data exhibited a significant low-frequency oscillation around zero. The standard deviation of the oscillation is approximately 25 nm ($1x10^{-6}$ in), and the frequency of oscillation is approximately within the range 0.10 to 0.15 Hz. Unfortunately, the present study did not afford the time to characterize the low-frequency oscillation of the displacement transducers more accurately, and to develop a custom filter to compensate for the effect.

### Hysteresis Calculations

To quantify the magnitude of hysteresis present in the data, while minimizing the error introduced by the displacement measurement oscillations, the final averaged load-cycle data were passed through a numerical integrator to compute the energy loss during load cycling. Integrating the averaged load times the averaged displacement around the entire load-cycle resulted in a calculation of the total energy loss within the hysteresis loop. This final data-reduction step can be thought of as another form of data filtering in which the low-frequency oscillations in the displacement data are averaged out over the entire hysteresis loop. In order to compare results obtained at different load-cycle magnitudes, the total computed energy loss was normalized by the maximum elastic strain energy at the given load-cycle magnitude (i.e., one-half times the product of the maximum load and the maximum displacement).

## Test Results

As mentioned in the last section, each test specimen was load cycled between tension and compression load limits of: 44.5; 66.8; 89.0; 111.3; 133.5; 178.0; 222.5; 267.0; 356.0; and 445.0 N (10, 15, 20, 25, 30, 40, 50, 60, 80, and 100 $lb_f$). To generate statistically significant results, each specimen was tested six times at most load-cycle magnitudes (four times at the highest two load-cycle magnitudes). Data from each test were filtered and numerically integrated to compute energy loss under load cycling. Results from multiple tests on a single specimen at each load-cycle magnitude were used to estimate mean energy-loss values and standard deviations. The resulting data are presented in the following sections.

### Micro-slippage in the Press-Fit Pin: Results from the Calibration Specimens

The energy loss per load cycle is presented in Fig. 13 for the three calibration specimens. As explained previously, C-0 was a solid aluminum rod which exhibited approximately the same axial stiffness as the revolute joint specimens. C-a and C-b were identical to the joint specimens except the bearing assembly (see Fig. 2a) was replaced with a solid piece of aluminum. C-a was assembled with the high-press-fit pin, and C-b was assembled with the low-press-fit pin (see Table 1).

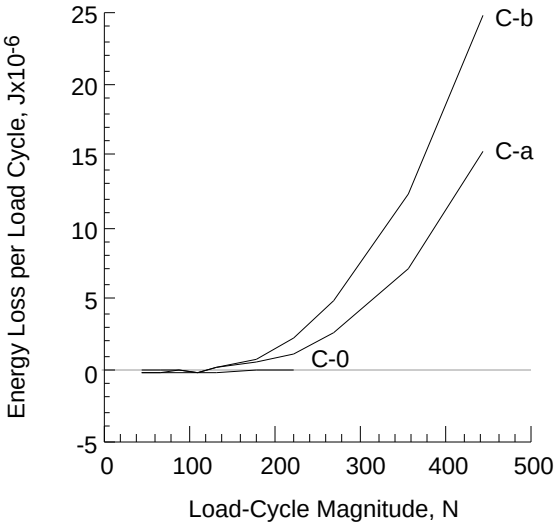


**Fig. 13 Total energy loss.**

As expected, C-0 (the solid aluminum rod) exhibits no significant hysteretic energy loss. Due to its limited buckling strength, C-0 was not tested at load-cycle magnitudes above 223 N (50 $lb_f$). Nevertheless, the data from C-0 serve to validate the present test setup, instrumentation, and data reduction algorithms.

Both C-a and C-b exhibit no significant hysteretic energy loss at load-cycle magnitudes less than 100 N (22 $lb_f$). Apparently, friction-induced microslippage at the surface of the press-fit pin is negligible within this load range, and both specimens exhibit essentially perfectly elastic response to load cycling.

Both C-a and C-b exhibit significant energy loss at load-cycle magnitudes greater than 100 N (22 $lb_f$), with C-b exhibiting approximately 60-70% more energy loss than C-a. This result indicates that the high-press-fit pin incorporated in C-a is more resistant to localized friction-induced micro-slippage than the low-press-fit pin incorporated in C-b.

### Low-Magnitude Bias Error in Data

To better visualize the energy-loss results at low-load-cycle magnitudes, the data presented in Fig. 13 are presented in Fig. 14 with the ordinate expanded by a

factor of five. In this plot, it is evident that the calculated energy loss is slightly negative for all calibration specimens at load-cycle magnitudes below 120 N (26 $lb_f$), which, of course, is impossible. This artifact might be due to a temporal bias error in either the load or displacement data. For example, a slight shift of the load-response data forward in time relative to the displacement-response data would appear as a negative hysteresis in the load-displacement response.

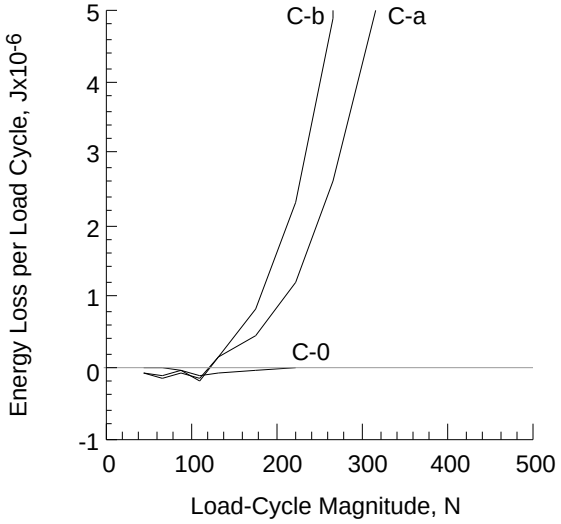


**Fig. 14 Total energy loss.**

One possible source of the bias error is the numerical filtering algorithm employed herein to filter high-frequency noise from the raw data signals. As mentioned previously, filtering algorithms are essentially numerical integrators, and many algorithms tend to induce artificial temporal shifts in the filtered data. Although the present filtering algorithm is specifically designed to introduce no bias errors, a simple test was performed to verify the algorithm's performance. The raw data from C-b was passed through the energy-loss-calculation algorithm and compared with the results generated using the filtered data. This comparison is presented in Fig. 15. Only slight discrepancies exist between the energy-loss calculations generated using the raw and filtered data, and both raw and filtered data result in the negative-energy-loss calculations at low load-cycle magnitudes. This comparison indicates that the high-frequency filtering algorithm introduces no significant bias errors, and has little effect on the energy-loss calculations.

A number of other possible sources of bias error were identified and systematically investigated in an effort to correct the problem. To date, no explanation has been found for the error, but its absolute magnitude is quite small (i.e., on the order of $0.6 \times 10^{-6}$ J), and its effects are only noticeable in the energy-loss calculations at low-load cycle magnitudes.

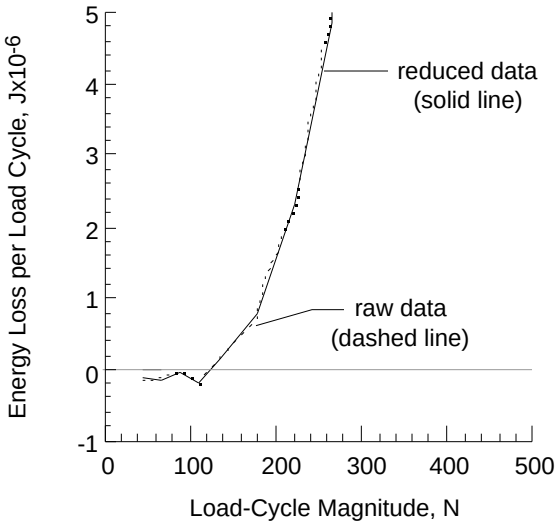


**Fig. 15 Comparison of energy-loss calculation using raw and reduced data from C-b.**

Unfortunately, the bias error makes it impossible to discriminate a precise load-cycle magnitude below which micro-slippage ceases to occur. In other words, the present data do not prove whether friction-induced micro-slippage in the press-fit pin asymptotically approaches zero at zero load-cycle magnitude, or effectively vanishes at some finite load-cycle magnitude.

### Percent Energy-Loss Calculations and Random Data Errors

To provide a better basis for comparison of results derived at different load-cycle magnitudes, energy loss is normalized by the total elastic strain energy at the given load-cycle magnitude. To illustrate this procedure, the energy-loss data presented in Fig. 13 are normalized and presented as percent-energy-loss data in Fig. 16.

Since normalizing involves dividing the energy loss by the square of the load-cycle magnitude, errors in the energy-loss calculations are also divided by the square of the load-cycle magnitude. Thus, errors in the energy-loss data appear to be greatly magnified in the percent-energy-loss data at low-load-cycle magnitudes. For example, the bias error identified in the last section has a substantially greater effect on the percent-energy-loss calculations at low-load-cycle magnitudes than it does at high-load-cycle magnitudes. Hence, the slightly negative energy-loss calculations at low load-cycle magnitudes become greatly exaggerated when normalized to percent energy loss.

Also included in Fig. 16 are the estimated one-standard-deviation error bars associated with random

variability in the percent-energy-loss calculations for C-b (note: the error bars for the other two specimens were comparable in magnitude and are omitted for clarity). These error bars were determined from statistical variation in the results derived from six tests performed at each load-cycle magnitude. By definition, these error bars do not include the aforementioned bias error, because they are derived assuming the data from the six tests represent a normally distributed population. Therefore, these error bars represent the effects of all other sources of error that are random by nature. In general, the percent-energy-loss data exhibited reasonably small random variability. However, the variability was slightly greater at low-load-cycle magnitudes.

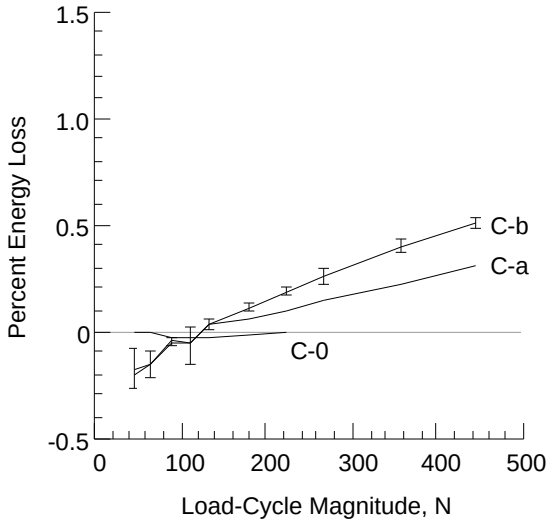


**Fig. 16 Percent energy loss.**

### Micro-slippage in the Bearings: Results from the Revolute Joint Specimens

Results from percent-energy-loss calculations performed on data from specimens J-a-05, J-b-05, J-a-20, and J-b-20 are presented in Fig. 17. Comparing these results with those presented in Fig. 16 for C-a and C-b, it appears that specimens J-a-05, J-b-05, J-a-20, and J-b-20 exhibit between two and three times the hysteretic energy loss as specimens C-a and C-b. Hence, it is concluded that roughly the same amount of friction-induced micro-slippage occurs within the bearing and as occurs within the press-fit pin under load cycling.

Comparing results from specimen J-a-05 with those from J-b-05 and results from specimen J-a-20 with those from J-b-20, it appears that the specimens with high-press-fit pins (J-a-05 and J-a-20) exhibit less micro-slippage (and energy loss) under load cycling than the specimens with low-press-fit pins (i.e., J-b-05 and J-b-20). This trend is consistent with the results presented in Fig. 16 for specimens C-a and C-b. Likewise, the specimens with high-preload bearings (i.e., J-a-20 and J-b-20) ) exhibit less micro-slippage (and energy loss) under load cycling than the specimens with low-preload bearings (i.e., J-a-05 and J-b-05).

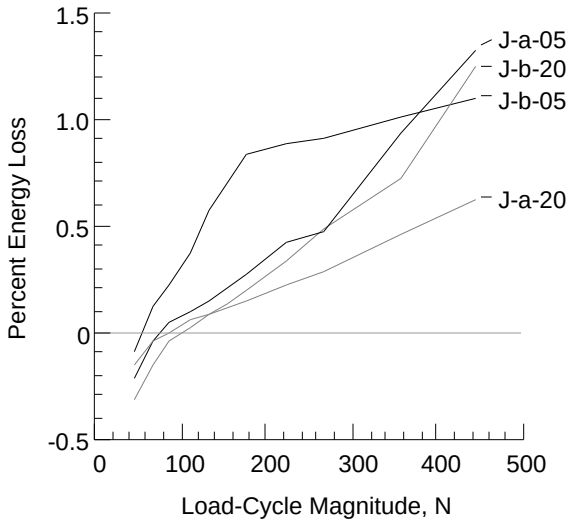


**Fig. 17 Comparison of bearing preload and pin press-fit effects.**

All specimens summarized in Fig. 17 exhibit monotonically increasing energy loss with increasing load-cycle magnitude. The shapes of the curves for specimens J-a-05, J-a-20, and J-b-20 are fairly similar, however the curve for specimen J-b-05 (i.e., the specimen with the lowest bearing preload and lowest pin press-fit) is dramatically different. Specimen J-b-05 exhibits a much more rapid increase in energy loss than the other specimens as the load-cycle magnitude is increased from 100 N (22 $lb_f$) to 200 N (45 $lb_f$).

One possible explanation for this response is increased micro-slippage at low-load-cycle magnitudes due to non-conformability between the various pin and bearing interfaces. Conformability is defined as the extent over which two contacting surfaces physically touch one another (e.g., the amount of physical contact between a ball and a race within the bearing). Lightly-preloaded interfaces (such as those in specimen J-b-05) tend to conform poorly due to manufacturing defects in the mating surfaces. However, heavily-preloaded interfaces (such as those within specimen J-a-20) are more likely to conform due to local elastic deformations which accommodate manufacturing defects.

To further assess the effects of manufacturing variability, five nominally identical specimens were tested (specimens J-b-10 described in Table 1). These specimens incorporated mid-preload bearings and low-

press-fit pins. The results of percent-energy-loss calculations for these specimens are presented in Fig. 18.

There is significant variation in the results from different specimens. Part of this variation is attributable to the 50% uncertainty in bearing preload and pin press fit (see Table 1). However, part of the variability in response is also likely attributable to variations in conformability between the many interfacing components. For example, two of the specimens exhibit a much more rapid increase in energy loss than the other specimens as the load-cycle magnitude is increased from 50 N (11 $lb_f$) to 150 N (33 $lb_f$) indicating poor conformability similar to that suspected to exist in specimen J-b-05.

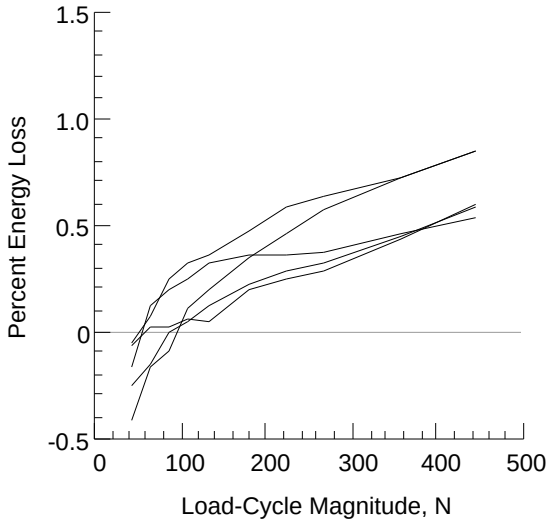


**Fig. 18 Variation in response due to manufacturing tolerances (specimens J-b-10).**

### Elastic Response at Low-Load-Cycle Magnitudes

Despite variability in actual response due to manufacturing tolerances, and uncertainties in energy-loss calculations due to an apparent bias error in the data, all specimens consistently exhibit negligible hysteretic energy loss at load-cycle magnitudes below 50 N (11 $lb_f$). Therefore, within the limitations of the present tests, all specimens exhibit no measurable friction-induced micro-slippage, and hence, perfect elastic response to quasi-static load-cycling at these low load-cycle magnitudes.

Recall that the simple model used in Ref. 5 to predict micro-lurching in the deployable metering truss implicitly assumes that the joints in the metering truss exhibit linear elastic response under load cycling up to 33 N (7.5 $lb_f$) in magnitude. The present test data indicate that the joints, in fact, exhibit effectively elastic response up to approximately 50 N (11 $lb_f$) of load-cycle magnitude. Considering the simplicity of the model, this correlation is quite good. From a broader perspective, this correlation reinforces the assumption that friction-induced micro-slippage is responsible for both hysteretic response to quasi-static load cycling in the joints, as well as micro-lurching response to dynamic loading in the truss.

## Concluding Remarks

The present study has characterized the low-magnitude quasi-static load-cycle response of precision revolute joints incorporated in a deployable telescope metering truss. Attention has been focused on the hysteretic response of these joints because it is believed that hysteretic response to load cycling is caused by friction-induced micro-slippage at the interfaces between mechanical components within the joint. Furthermore, this micro-slippage is believed to be responsible for micro-lurching instabilities in the deployable telescope metering truss incorporating the joints.

Great care was taken in constructing the current test setup and data reduction procedures to minimize error sources. To quantify the magnitude of hysteresis present in the data, while minimizing the effects of noise in the data, total energy loss during load cycling was computed rather than measuring hysteresis width. Despite the many safeguards implemented to ensure accuracy in the results, it was found that a minor biasing error of unknown origin resulted in negative energy-loss calculations at low load-cycle magnitudes. As a consequence, the present data do not prove whether friction-induced micro-slippage in the precision revolute joint asymptotically approaches zero at zero load-cycle magnitude, or vanishes at some finite load-cycle magnitude.

Data indicate that approximately the same amount of micro-slippage (i.e., hysteretic energy loss) occurs in both the angular-contact bearing that allows rotation of the joint, and the press-fit pin that is used to affect final assembly of the joint. It was also found that the amount of micro-slippage-induced hysteresis generally decreases as bearing preload is increased and/or pin press-fit is increased.

Five specimens having nominally the same bearing preload and pin press-fit exhibited fairly significant variation in their hysteretic response. This variability in response is partly attributable to the 50% uncertainty in bearing preload and pin press fit, and partly attributable to variations in conformability between the many interfacing components within the specimens.

Finally, it was shown that all specimens exhibit negligible hysteresis in response to load cycling of up to approximately 50 N (11 $lb_f$) in magnitude. This

result was correlated with results from a simplified system-response model developed in Ref. 5 to predict micro-lurching response in the deployable telescope metering truss test article. This correlation reinforces the assumption that friction-induced micro-slippage is responsible for both hysteretic response to quasi-static load cycling in the joints, as well as micro-lurching response to dynamic loading in the truss.

## References


[1]Peterson, L. D., et al., "Micron Accurate Deployable Antenna and Sensor Technology for New-Millennium-Era Spacecraft," presented at the 1996 IEEE Aerospace Applications Conference, Snowmass, Colorado, February, 1996.

[2]Bullock, S. J., and Peterson, L. D., "Nonlinear Micron-Level Mechanics of a Precision Deployable Space Structure Joint," presented at the 37th AIAA/ ASME/ASCE/AHS/ASC Structures, Structural Dynamics, and Materials Conference, Salt Lake City, UT, April 15-17, 1996.

[3]Lake, Mark S., Warren, Peter A., and Peterson, L. D., "A Revolute Joint with Linear Load-Displacement Response for Precision Deployable Structures," presented at the 37th AIAA/ASME/ASCE/AHS/ASC Structures, Structural Dynamics, and Materials Conference, Salt Lake City, UT, April 15-17, 1996.

[4]Warren, Peter A., and Peterson, L. D., "Experimental Characterization of the Nonlinear Post-Deployment Micro-Mechanics of Precision Deployable Space Structures," presented at the 37th AIAA/ASME/ASCE/ AHS/ASC Structures, Structural Dynamics, and Materials Conference, Salt Lake City, UT, April 15-17, 1996.

[5]Warren, Peter A., "Sub-Micron Non-Linear Shape Mechanics of Precision Deployable Structures," Ph.D. Dissertation, University of Colorado, 1996.